

Analyzing Properties of Monolayer MoS₂ Using RHEED and Ultrafast Electron Diffraction

Calvin Chiu¹, Thomas Liang², Xing He[#] and Ding-Shyue Yang[#]

¹Klein Cain High School, USA

²Dawson High School, USA

[#]Advisors

[°]These authors contributed equally to this work

ABSTRACT

Reflection high-energy electron diffraction (RHEED) and ultrafast electron diffraction (UED) are techniques used to characterize crystal structures both statically and dynamically. These experimental methods are of academic interest due to their ability to visualize crystal structures on the atomic level and analyze dynamic changes on the picosecond scale. In this experiment, RHEED and UED are implemented to analyze monolayer molybdenum disulfide (MoS₂), a compound that may contribute to the future of microelectronics. Images of various diffraction patterns are presented, and analysis is conducted on diffraction peaks, lattice spacing, and photoinduced intensity changes.

Introduction

Monolayer molybdenum disulfide is part of a group known as 2D transition-metal dichalcogenides (TMDCs). These materials can function as semiconductor transistors, and their 2D structures contribute to favorable electronic properties^{1,2}. As a result, they may potentially replace other materials for future use in computer chips, flexible electronics, and energy harvesting^{2,3,4}. Monolayer MoS₂ is one of the more valuable materials in this family due to its direct band gap of 1.8 eV, so analysis of its properties can provide valuable information for the next generation^{2,5}.

This experiment utilizes reflection high-energy electron diffraction (RHEED) and ultrafast electron diffraction (UED) in reflection geometry to analyze certain properties of molybdenum disulfide. The use of electron diffraction rather than conventional optical spectroscopy allows for greater resolution on the picosecond scale⁶. RHEED involves directing an electron beam onto a sample such that diffraction patterns produced on a phosphor screen are measured⁷. Ultrafast electron diffraction (UED) uses a time-resolved pump-probe technique by exciting the sample through an optical laser (pump) and directing an electron beam onto the sample (probe), resulting in a diffraction pattern^{8,9,10}. Data is collected by the machine at different times relative to the photoexcitation. Both RHEED and UED allow for a fundamental understanding of molybdenum disulfide's atomic structure and photoinduced dynamics^{11,12}.

Results and Discussion

Visualization of Changing Tilt Angle

Data from 221 tilt angles were collected and outputted as images using RHEED (Fig. 1). From the images, several important points are noted. First, the Bragg peaks are represented as streaks rather than spots, which is consistent with the expected RHEED pattern for a monolayer⁸. Each streak is roughly the same distance apart from adjacent streaks. The different tilt angles clearly show the magnitude of the general intensity of diffraction peaks, with the 2nd and 3rd images having the greatest Bragg peaks.

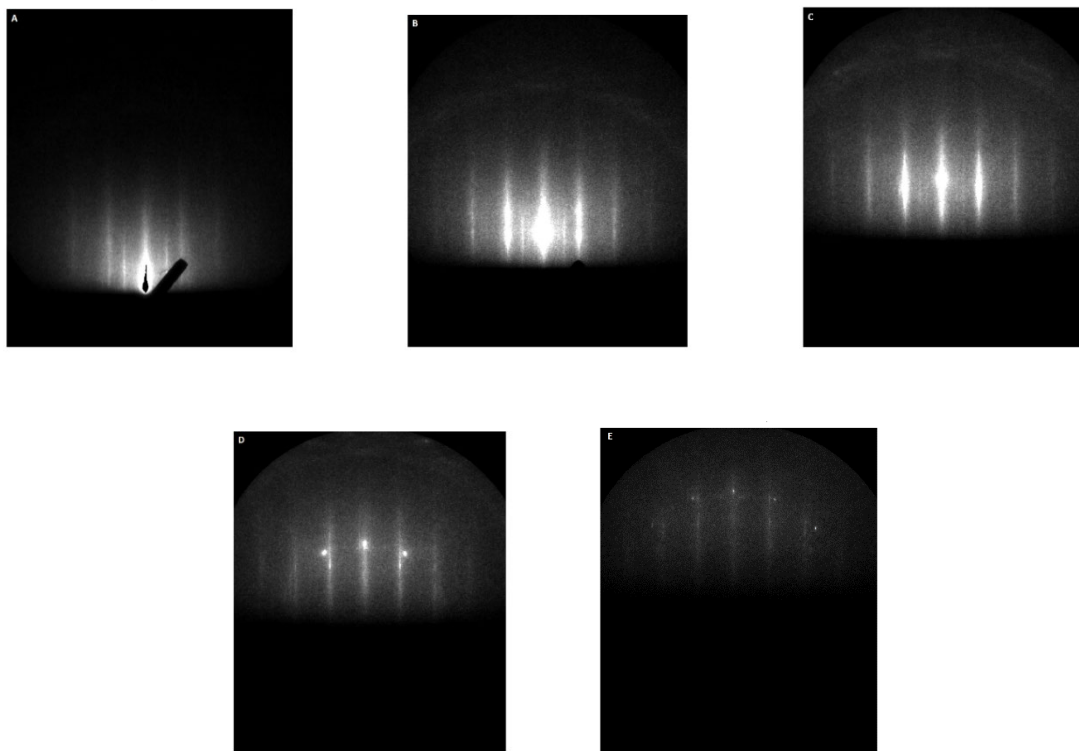


Fig. 1 Selected images of different tilt angles. Tilt angle is increased from image A to image E. Brighter spots indicate higher intensity and thus greater constructive interference.

Lattice Constant Calculation

To calculate the lattice constant from the images, we first create a horizontal intensity plot from image C (Fig. 1). We choose a horizontal axis slightly below the axis with the highest brightness to avoid oversaturation factors (extreme intensity peaks that may impact the profile shape). The horizontal intensity plot is shown in Fig. 2.

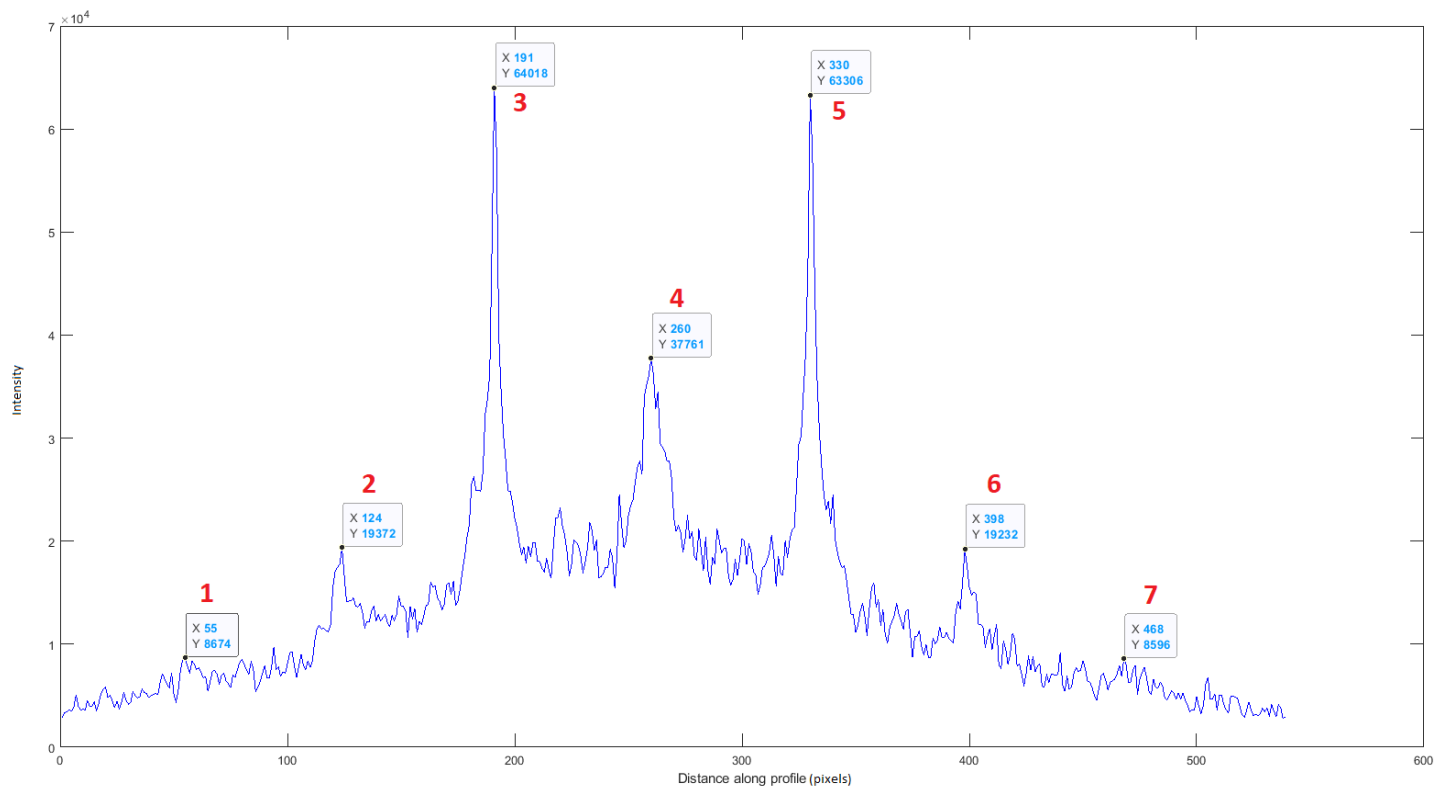


Fig. 2 Intensity is plotted as a function of the distance along the horizontal profile from left to right. Data points are selected to indicate the relative peaks of intensity along the profile.

From the image, the lattice constant can be calculated using the distance between adjacent peaks. The pixel difference between peaks 3 and 4 is 69 pixels. Using this pixel difference, the momentum transfer Δk associated with these diffractions is calculated to be 0.365 \AA^{-1} . This Δk value results in a calculated lattice constant value of 3.167 \AA . Thus, the lattice constant calculated by RHEED in this experiment is within the literature value of 3.15 \AA ¹³.

Alternatively, the distance between peaks 3 and 4 and peaks 4 and 5 can be averaged. The average pixel separation between these peaks is 69.5 pixels. Using the same method from above, the calculated lattice constant is 3.145 \AA , which is also consistent with the literature value of 3.15 \AA ¹³. The averaged value for the spacing between adjacent streaks helps to reduce some asymmetry in the intensity profile.

Another method to find the lattice constant would be to use curve fitting, which is more accurate because it identifies the centers of the peaks to the accuracy of a fraction of a pixel. One example of a curve fit is to use a Gaussian function, as shown in Fig. 3. The properties of the Gaussian curves for peaks 3, 4, and 5 are shown in Table 1, and the curve fits for the peaks are shown in Fig. 4. Using the horizontal distance between peaks 3 and 4, the lattice constant was determined to be 3.154 \AA . With peaks 3 and 4 and peaks 4 and 5 averaged together, the lattice constant found was 3.142 \AA . These calculations are also consistent with the literature value, showing that the Gaussian fit provides a good determination of the peak positions on the intensity plot. However, a Lorentzian function may be used to provide a better overall fit, as it includes the tail parts of the diffraction peak as part of the curve.

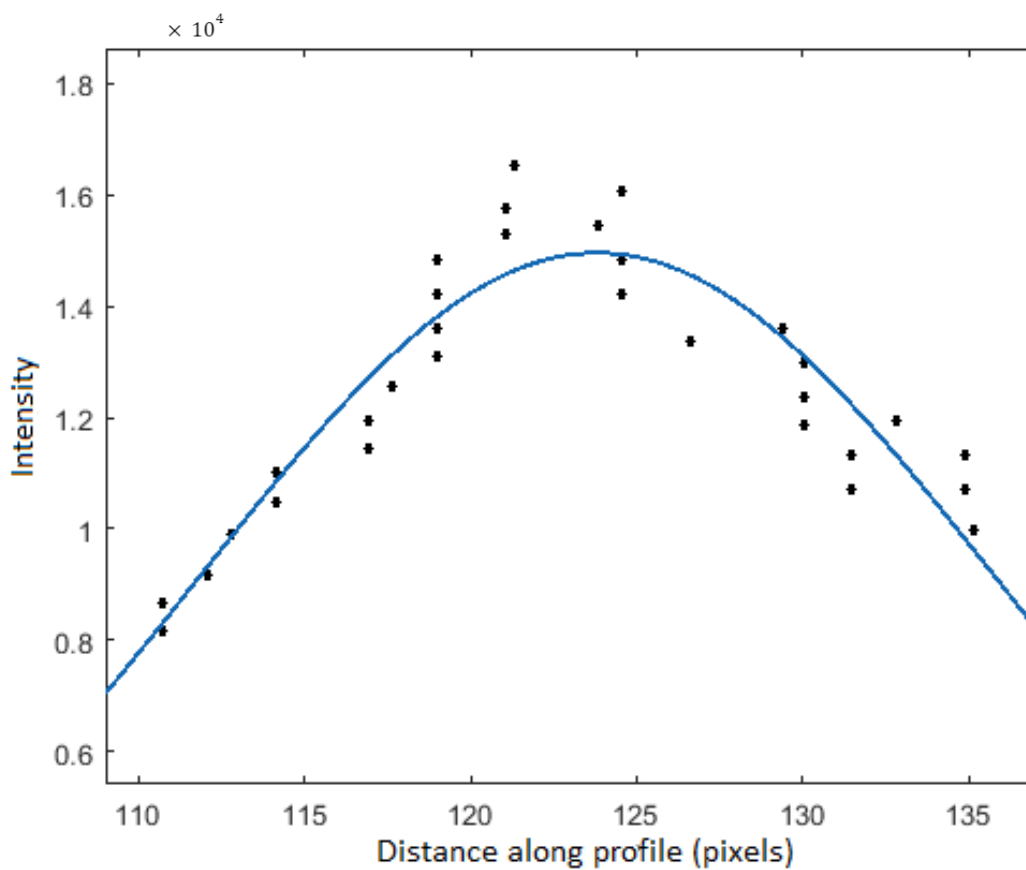


Fig. 3 The Gaussian curve fit applied to peak 2 of Fig. 2.

Table 1 Variables of the Gaussian curves for peaks 3, 4, and 5.

	Peak 3	Peak 4	Peak 5
a (amplitude of peak)	3.793 ± 0.122	1.580 ± 0.176	3.892 ± 0.123
b (peak distance along horizontal profile)	189.4 ± 0.10	258.7 ± 0.60	328.5 ± 0.10
c (width of peak)	3.162 ± 0.163	6.110 ± 0.936	3.349 ± 0.140

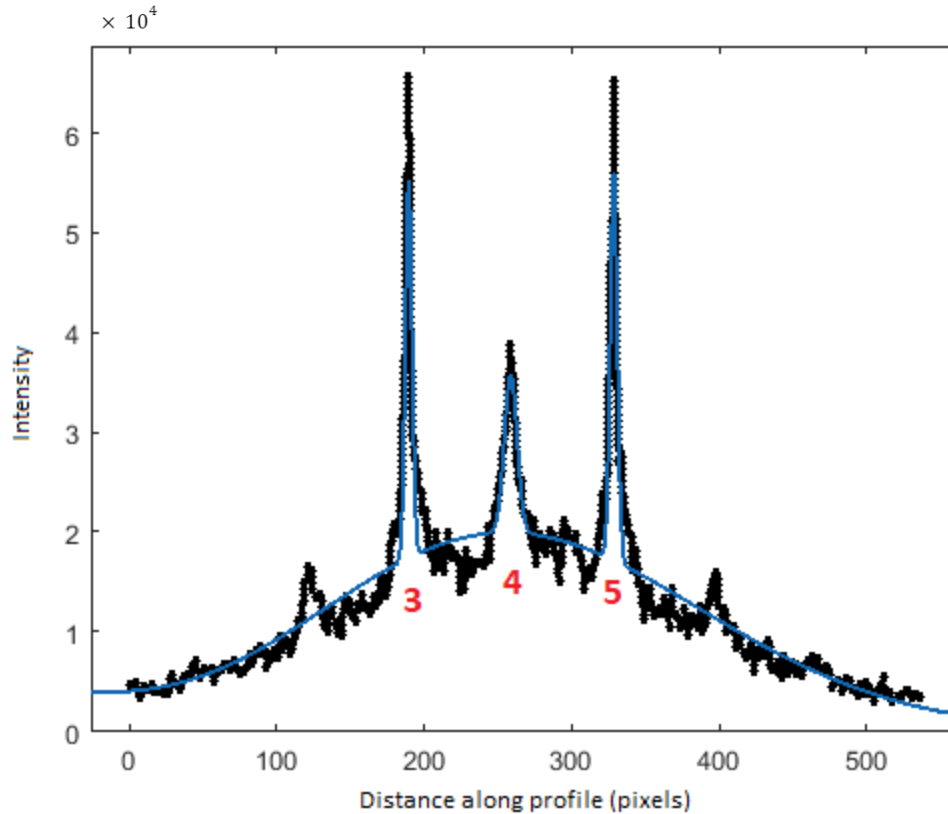


Fig. 4 Gaussian curve fits for peaks 3, 4, and 5.

Rocking Curve

Next, we analyze the data through the use of the rocking curve, which provides a general visualization of the change in the diffraction patterns over the electron incidence angle. The rocking curve plots the intensity of the y-axis as a function of the incidence angle, whose concept is also often seen in X-ray diffraction (XRD) for thin films and other materials^{14,15}. A narrow vertical strip is taken as the region of interest, in this case the central bright spot of the images. The strip is compressed into a 1-pixel wide strip, and each strip is added to the next for each tilt angle, which creates the desired rocking curve (Fig. 5).

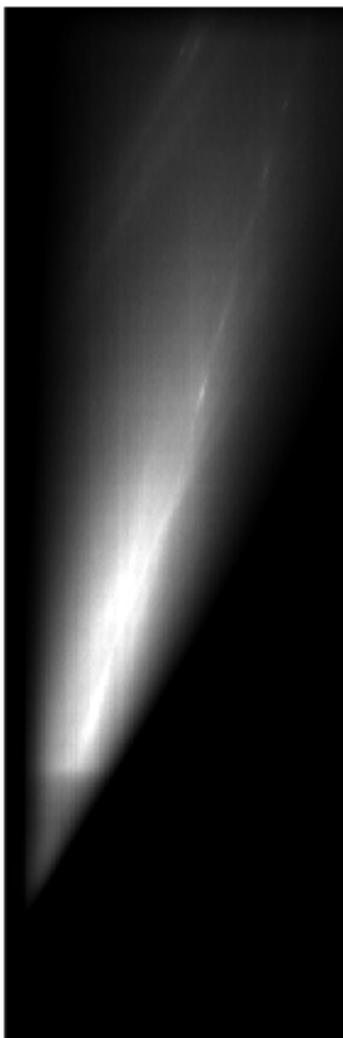


Fig. 5 The rocking curve for molybdenum disulfide. The region of interest is seen as moving “up” within the vertical strip as the tilt angle is increased. Thus, the diffraction pattern of MoS₂ is visualized more thoroughly through the rocking curve.

The rocking curve allows for further analysis of the structure of MoS₂. The mean intensity for a given tilt angle is determined by averaging the overall intensity along the vertical length of the rocking curve. Next, the axis of the incidence angle is converted into a quantity known as the “scattering vector,” which represents the difference between the direct and reflected electron beams in reciprocal space. The mean intensity is graphed as a function of the scattering vector (Fig. 6). The plot shows that for a certain scattering vector (around 1.5 inverse angstroms), there is a high diffraction intensity. Thus, the specific tilt angle that corresponds to that scattering vector is the optimal angle for identifying diffraction peaks.

Furthermore, a diagonal profile can be created from the rocking curve (Fig. 7). The resultant plot is used to identify the higher-order Bragg peaks along the diagonal¹⁶. The almost featureless intensity evolution without multiple identifiable peaks over the incidence angles further shows that the MoS₂ sample is indeed a monolayer.

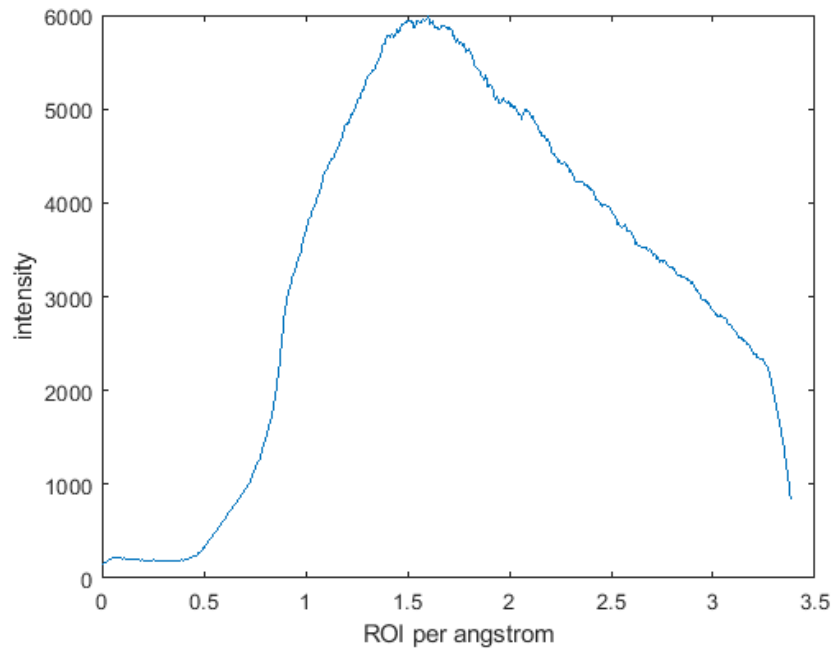


Fig. 6 The plot of intensity vs the scattering vector in reciprocal space.

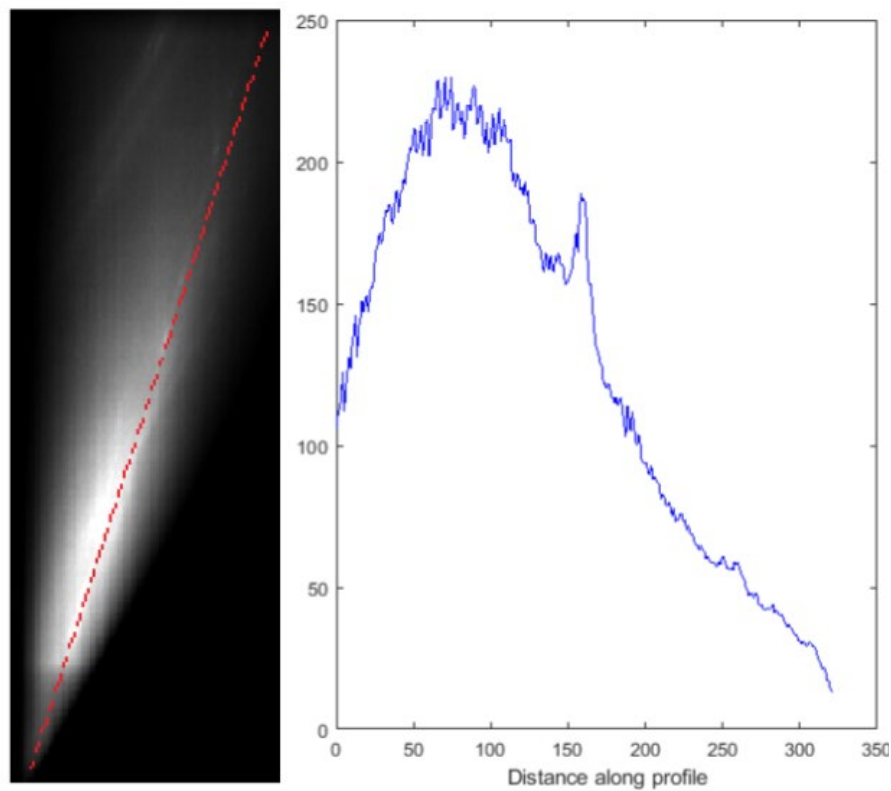


Fig. 7 A diagonal profile, shown in red, is taken along the rocking curve to catch the diffraction peaks near the upper right corner. The plot is created of intensity as a function of the distance along the profile (from bottom left to upper right). The peaks after a distance of 150 pixels along the profile correspond to the aforementioned diffraction peaks.

Azimuthal Scan Visualization

Similar to the data from various tilt angles, data from 90 different azimuthal angles were collected and outputted as images (Fig. 8).

The azimuthal scan is useful because it allows for the identification of many features of monolayer MoS₂. The circular spots that rotate through the images represent the diffraction patterns of the sapphire substrate underneath the MoS₂ monolayer¹⁷. Faint semicircle patterns near the top of the images represent the first-order Laue zones¹⁸. Finally, the lines streaking outwards in some of the images represent Kikuchi lines¹⁹.

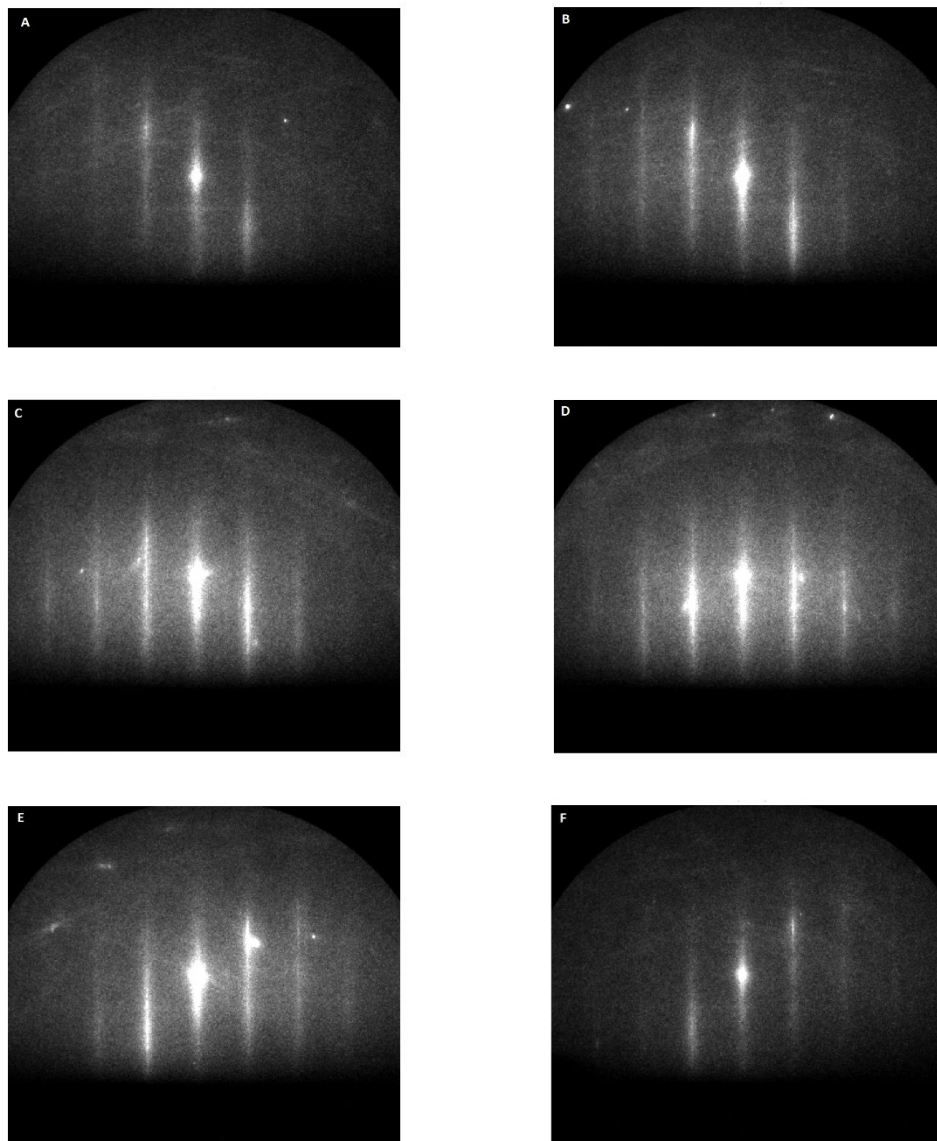


Fig. 8 Chosen images from the azimuthal scan of MoS₂. The diffraction pattern is seen as “rotating” as the azimuthal angle is changed. Various other features are noted as described above.

In addition, the azimuthal scan allows for the visualization of the orientation of monolayer MoS₂ with respect to the supporting surface's lattice. The streaks together form a hexagonal structure, and since a hexagonal structure in reciprocal space is also a hexagonal structure in real space²⁰, we conclude that monolayer MoS₂ is hexagonal. Overall, the images support the crystalline nature of the monolayer and its good azimuthal relation with the supporting substrate.

Ultrafast Electron Diffraction

In the UED analysis of MoS₂, a total of 20 scans are conducted. Each scan has a collection of data that correspond to images of the diffraction patterns at different electron-probing times (relative to the photoexcitation by the laser). After checking if there are any outlier scans from unwanted background noise, a matrix is created that stores the average image appearance for all the scans combined. Thus, images are produced for each specific time (Fig. 9).

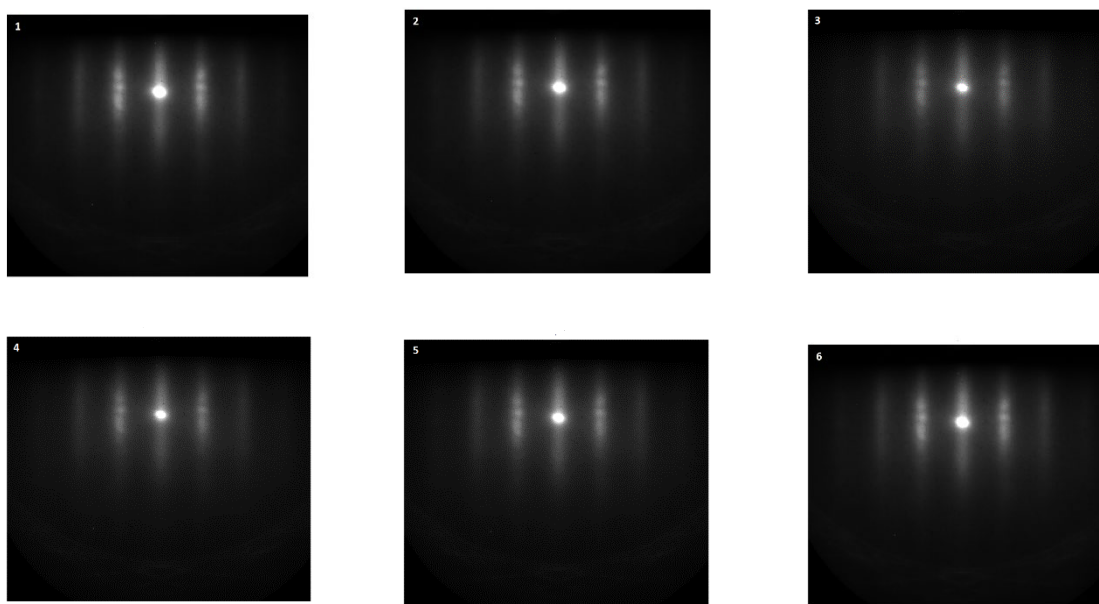


Fig. 9 Selected images of the average of the combined scans. Time 1 is from before photoexcitation, times 2 and 3 are during photoexcitation, and times 4-6 are during the relaxation process, as seen by the brightness of successive images. Times of images 1-6, in picoseconds, are -9.3, 0.7, 10.7, 20.7, 58.7, and 138.7.

Although the images appear similar by appearance, numerical analysis can be conducted to visualize how the lattice responds to the photoexcitation. A region of interest (ROI) is selected, and the ROI intensity is averaged for all the pixels in the region. Thus, a single intensity value is created for each time. Since the highest intensity occurs around the first 5 time intervals (because photoexcitation has not yet occurred), an intensity ratio is calculated as the ROI mean intensity for a given time divided by the highest intensity. A graph of the intensity ratio as a function of time is created (Fig. 10).

For each region of interest that corresponds to a relatively high-intensity peak, a background region of interest is also chosen. This background region provides a “reference” as to how the bright ROI changes compared to the regions around it. Two sets of ROIs are shown in Fig. 10 and 11.

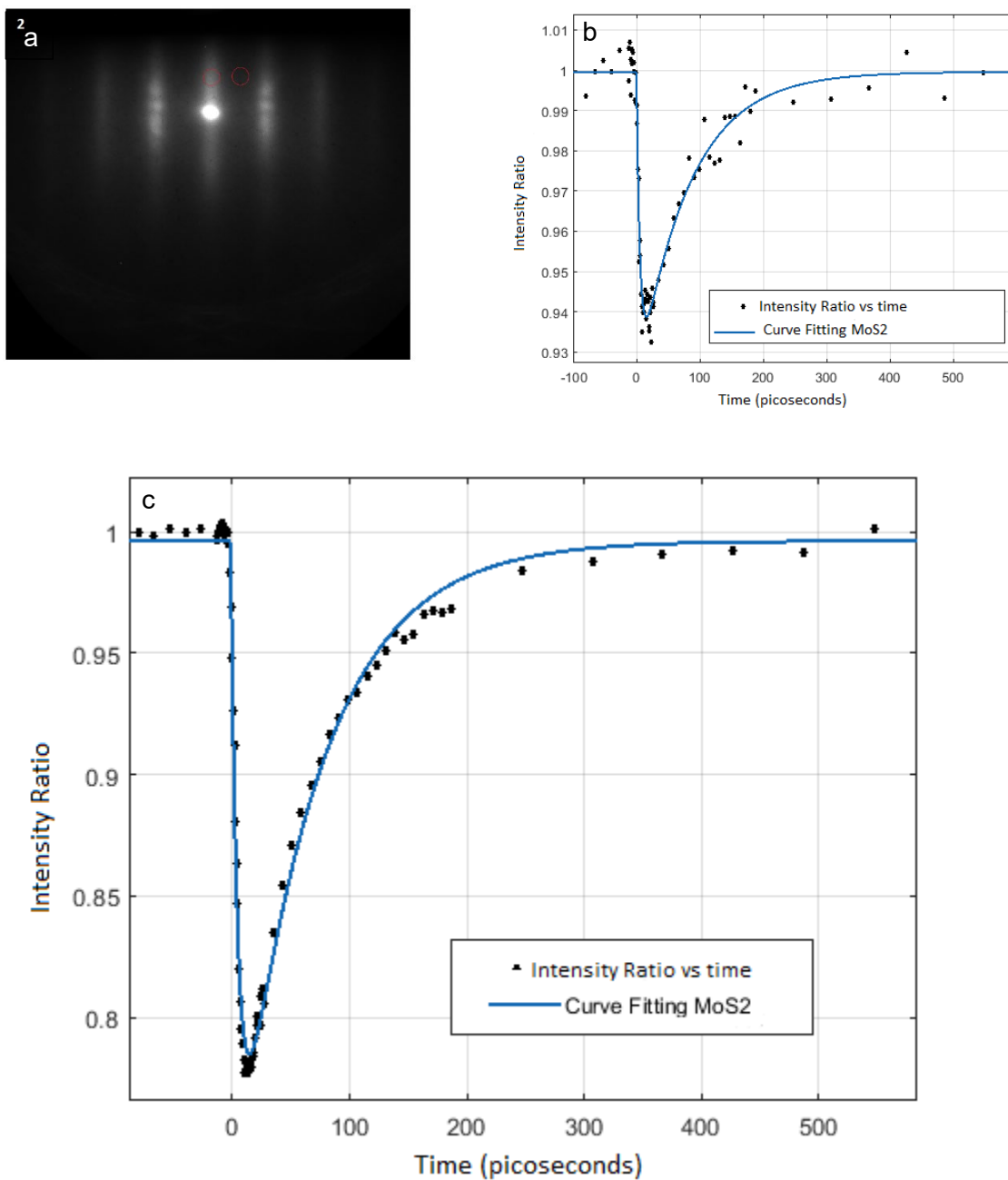


Fig. 10 a) The regions of interest shown on time 2, with red as the peak ROI and blue as the background ROI. The central bright peak is avoided due to oversaturation. c) The intensity ratio as a function of time for the background ROI. b) The intensity ratio as a function of time for the peak ROI.

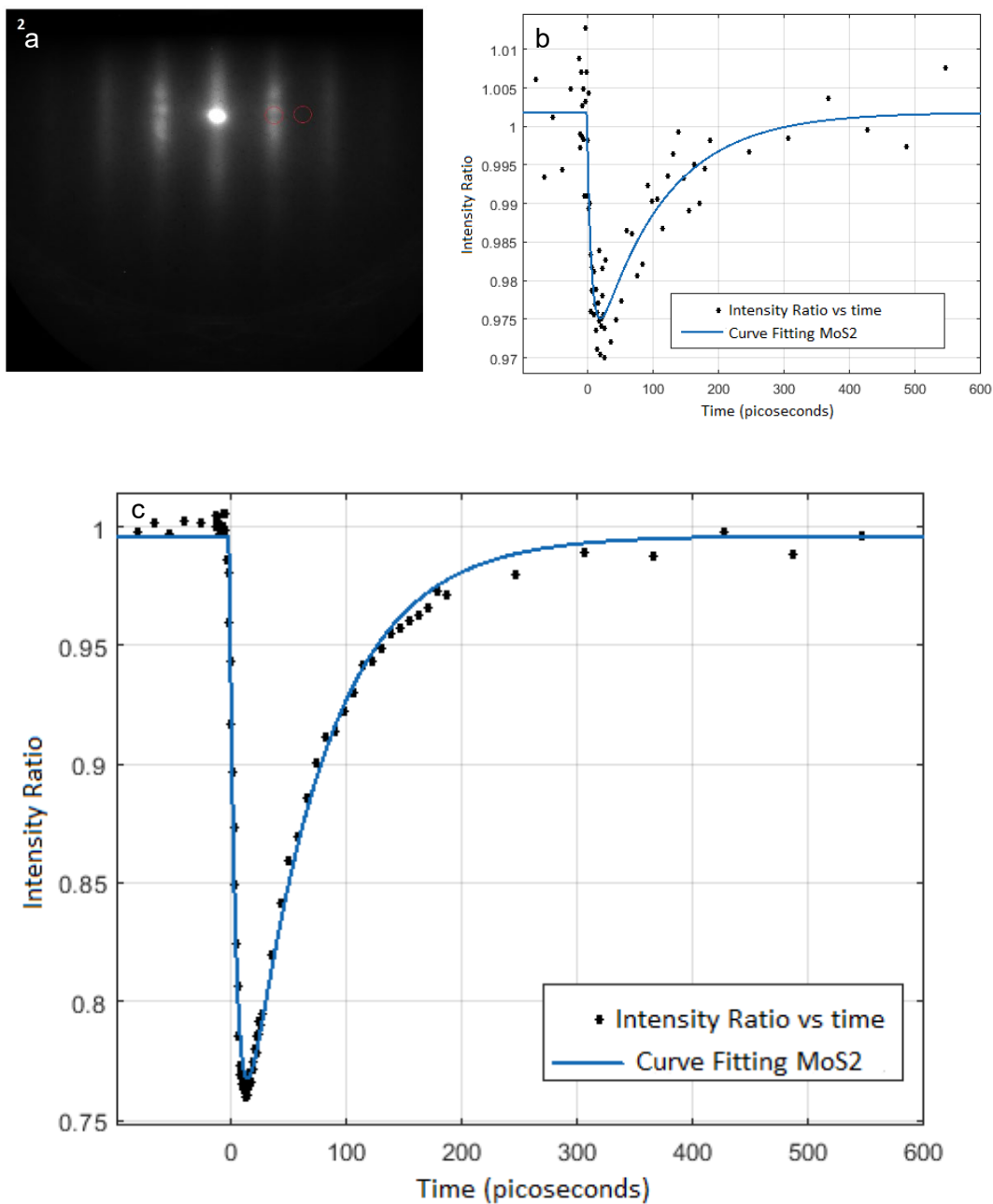


Fig. 11 Similar figures as Fig. 10 for a different set of ROIs.

These graphs are used to analyze how photoexcitation influences MoS₂. From Fig. 10, the peak ROI is seen to drop near 0.75, meaning that the average intensity of the region decreased by almost 25% as a result of photoexcitation. After excitation, the crystal lattice takes time to go back to its original state during the relaxation process, and the intensity comes back to its original value in approximately 400 picoseconds. The background plot exhibits a similar pattern. However, the data points appear more scattered, which is likely due to a smaller signal-to-noise ratio. Moreover, the background intensity ratio only decreases by about 6%, much less than the decrease from the peak ROI. However, both the background and the peak ROI return to their original states at roughly the same time.

Fig. 11 shows similar characteristics as Fig. 10 with regard to the similarities and differences between the peak and background ROIs. The background ROI plot from the second set of data also has a lower signal-to-noise ratio. Moreover, the intensity ratio only decreases by about 2.5% due to the photoexcitation compared to the 6% from the first set.

Due to the similarities in properties such as electronic band properties, the photoinduced dynamics of molybdenum disulfide can be compared to that of gallium arsenide (GaAs). Data from gallium arsenide through UED has previously been collected¹⁶, and the results are shown in Fig. 12.

Comparing the intensity plots to that of MoS₂, it is seen that GaAs diffraction peaks decrease in intensity in a similar fashion. However, GaAs relaxes more quickly, as it reaches a plateau before 300 seconds for both the diffraction peak and background ROI. However, a full recovery to the original intensity (i.e, the intensity ratio returns to 1) is not complete within the observed temporal window, which means that gallium arsenide does not fully relax back to its original state within the time frame. Conversely, monolayer molybdenum disulfide reaches equilibrium in its original state sooner.

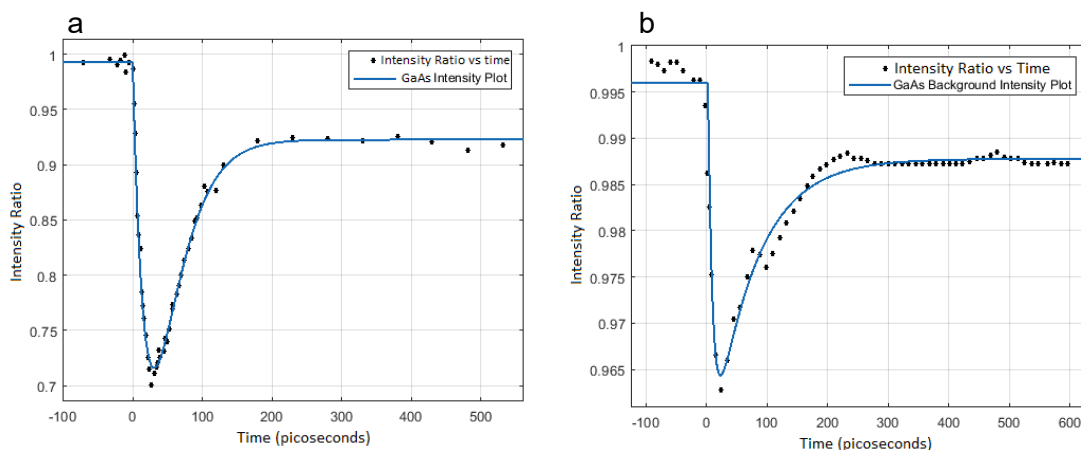


Fig. 12 Separate plots of the intensity ratio as a function of time for gallium arsenide.

Conclusion and Future Efforts

The use of electron diffraction techniques such as RHEED and UED allow for visualization of monolayer molybdenum disulfide's structures and dynamics. RHEED analysis techniques can be used to calculate the lattice constant, determine regions and angles with the highest diffraction intensities, and identify diffraction features in reciprocal space. UED provides information on how the crystal lattice responds to photoexcitation through visualizations and intensity plots.

Further analysis can be done on the structural features of MoS₂ as well as the intensity ratio plots of MoS₂ and GaAs. Furthermore, since this experiment was conducted under room temperature conditions and tested a specific set of incidence angles, future experiments can be done at various temperatures and a wider range of incidence angles. More information on these materials' structures and photoinduced dynamics may reveal important properties that affect their abilities to perform as efficient semiconductors.

Theory

Electron Wavelength

For electron diffraction to occur, the electron must be treated as a wave. From diffraction principles, the wavelength of the electron must be of similar magnitude as the interatomic distance between atoms in angstroms (Å) or 10^{-10} m. The wavelength is given by the de Broglie equation,

$$\lambda = \frac{h}{p} \quad \text{(Equation 1.1)}$$

where p is momentum and h is Planck's constant. In classical mechanics, the wavelength of the electron can be expressed in terms of energy,

$$\lambda = \sqrt{\frac{h^2}{2mE}} \quad \text{(Equation 1.2)}$$

where m is the electron mass²¹. However, for high-energy electrons, relativistic effects must be accounted for. The relation between kinetic energy and momentum can be written as

$$(E + m_0c^2)^2 = m_0^2c^4 + p^2c^2 \quad \text{(Equation 1.3)}$$

From this equation, the wavelength of the electron can be written as

$$\lambda = \sqrt{\frac{h^2}{2m_0E(1 + \frac{E}{2m_0c^2})}} \quad \text{(Equation 1.4)}$$

In this experiment, the electron energy is 30 keV, and the corresponding wavelength is 0.0698 Å. Thus, the above-mentioned requirement of the order of magnitude of the electron wavelength is satisfied.

Bragg Diffraction

The theory of electron diffraction stems from the concepts of Bragg diffraction, as shown in Fig. 13. When waves are incident upon a crystal, constructive interference occurs when an integer multiple of the wavelength equals the path difference between two given waves:

$$2d \sin\theta = n\lambda \quad \text{(Equation 2)}$$

Thus, when both the wavelength and the crystal lattice constant stay constant, altering the angle results in greater constructive or destructive interference.

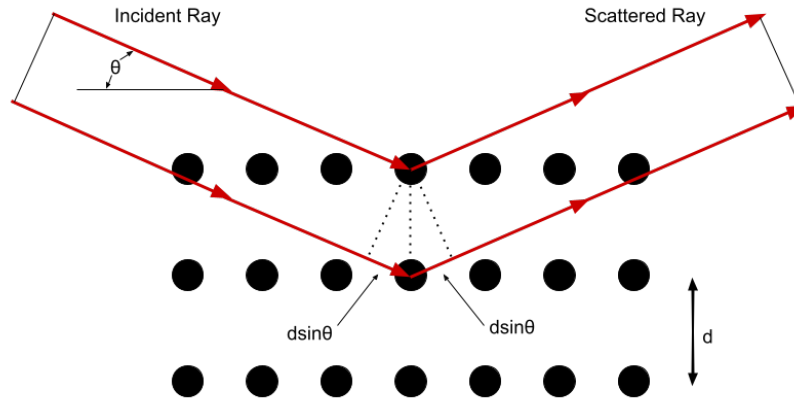


Fig. 13 A diagram of Bragg's law for coherent scattering of waves.

Reciprocal Space Theory and Laue Diffraction

Reciprocal space is created by taking the Fourier transform of a given crystal lattice, also known as a Bravais lattice²¹. This results in units being converted to their inverse counterparts, and it transforms the lattice into a more convenient form to use. The conversion of real space vectors to reciprocal lattice vectors is detailed in Equation 3.

A general description of diffraction is shown by the von Laue equations, which consider the beams as fields²². In this way, the diffraction patterns can be visualized in reciprocal space (Fig. 14).

$$b_1 = 2\pi \frac{a_2 \times a_3}{a_1 \cdot (a_2 \times a_3)}$$

$$b_2 = 2\pi \frac{a_3 \times a_1}{a_1 \cdot (a_2 \times a_3)}$$

$$b_3 = 2\pi \frac{a_1 \times a_2}{a_1 \cdot (a_2 \times a_3)}$$

Equation 3 The transformation of real space vectors to reciprocal lattice vectors through dot and cross products of vectors.

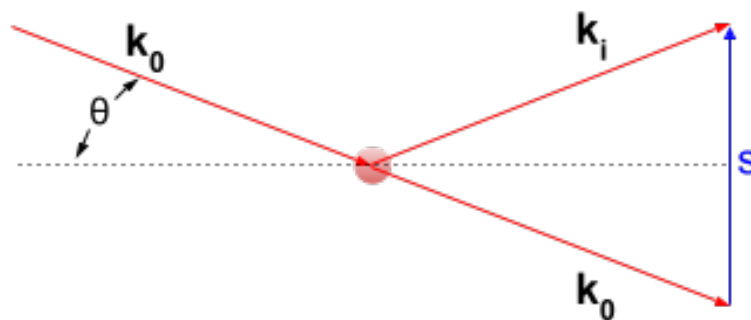


Fig. 14 The scattering process, based on the von Laue conditions.

Ewald Sphere and Reflection High-Energy Electron Diffraction (RHEED)

A theoretical construct known as the Ewald sphere is created to represent how the diffraction conditions arise in reciprocal space²³. An Ewald sphere with a radius of 90.0 \AA^{-1} is constructed for electron diffraction²². When a wave is incident on the crystal, both diffracted rays must constructively interfere to contribute to a Bragg peak¹². In reciprocal space, this corresponds to an Ewald sphere such that the reciprocal lattice vector intersects the surface of the sphere (Fig. 15).

Based on the nature of the crystal, different RHEED patterns will be projected onto a phosphor screen²⁴. When the Ewald sphere cuts the reciprocal lattice vectors with a monolayer crystal, a RHEED pattern consisting of streaks is seen (Fig. 16).

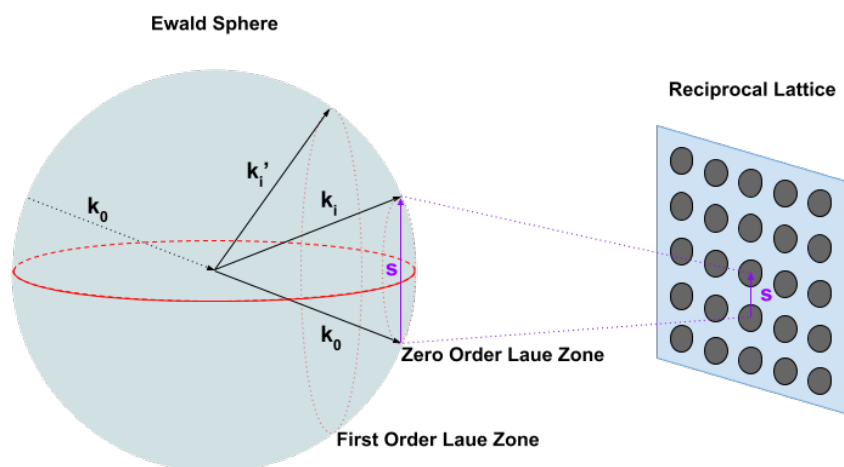


Fig. 15 The construction of the Ewald sphere in the 3D reciprocal lattice. Intersections between the sphere and the reciprocal lattice vector (s) correspond to diffraction peaks.

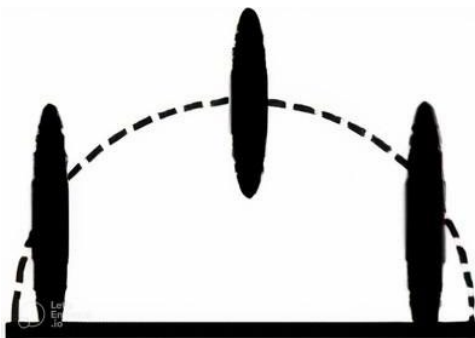


Fig. 16 The expected RHEED pattern, in reciprocal space, for a two-dimensional (monolayer) crystal.

Lattice Constant

By using reciprocal space imaging, one structural feature that can be determined is the lattice constant, which is the distance between unit cells in a lattice. We can convert from the peak-to-peak spacing to the lattice constant (Equation 4)²⁵. N_0 is the peak-to-peak spacing, b is the binning factor that accounts for the camera clustering adjacent pixels, m

is the number of microns per pixel, L is the camera length, Δk is the scattering vector in reciprocal space, k_0 is the length of the direct beam in reciprocal space (also equivalent to the inverse of the electron wavelength), c is a constant equal to $1/\sin 60^\circ$ (which is the angle between unit vectors in a hexagonal lattice), and a is the lattice constant.

$$d = n_0 \times b \times m \quad (\text{Equation 4.1})$$

$$\frac{d}{L} = \frac{\Delta k}{k_0} \quad (\text{Equation 4.2})$$

$$\Delta k = \frac{c}{a} \quad (\text{Equation 4.3})$$

Methods

In this experiment, we obtained an MoS_2 sample fabricated through chemical vapor deposition (CVD) from Professor Wen-Hao Chang's laboratory in Taiwan. Using a load-lock chamber and various transport mechanisms, the sample (Fig. 17) was loaded into the main chamber of the RHEED/UED apparatus (Fig. 18). The system was then pumped down to an ultra-high vacuum (2×10^{-10} torr) via a series of scroll, roughing, turbo, and ion pumps to reduce surface deterioration over time²⁶.

To supply electrons to target the MoS_2 sample, a 257.5 nm ultraviolet light beam was directed onto a sample of lanthanum hexaboride (LaB_6) within the electron gun. Electrons were emitted out of its surface via the photoelectric effect and were then accelerated to a kinetic energy of 30.0 kV and directed towards the MoS_2 sample.

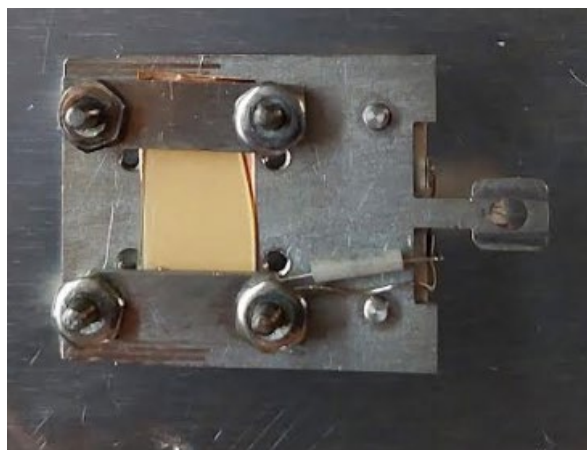


Fig. 17 The MoS_2 sample, created through chemical vapor deposition. The actual length of the sample is ~ 1.0 cm.

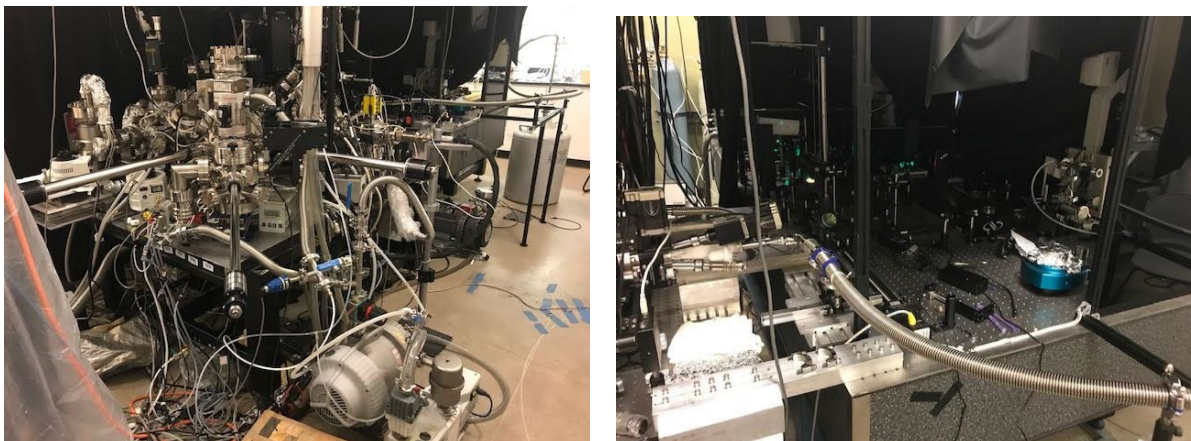


Fig. 18 Images of the RHEED and UED apparatus. a) View of the apparatus including the pumps, chambers, and electron gun. b) View of the optical setup used for the laser excitation during UED.

We first utilized RHEED to collect data regarding the sample. We vary 5 axes of motion: the 3 dimensions of x , y , and z as well as the tilting angle (w) and the azimuthal angle (t). The x , y , and z dimensions are initially changed to find the diffraction spots. As the electrons diffract from the sample, a diffraction pattern is created on a phosphor screen, which is translated by a camera into reciprocal space. In this experiment, the binning factor (b) is 4, the number of microns per pixel (m) is 6.5, the camera length (L) is 70500 micrometers, and the electron wavelength (λ) is 0.0698 angstroms. Data for various tilt angles are collected, and each tilt angle corresponds to a different magnitude of the intensity of the diffraction spots.

We then conduct an azimuthal scan to create other images of MoS_2 . After choosing the incidence angle, w , that optimizes the intensity of the diffraction peaks, data is collected by keeping w constant and changing the azimuthal angle, t .

To collect data regarding the dynamics of MoS_2 using UED in reflection geometry, we use an optical setup that allows light to be directed towards the sample (Fig. 19). By changing the wavelength, an infrared light source (1030 nm) is transformed into both visible light (515 nm) and ultraviolet light (257.5 nm). The UV light is used to eject electrons from LaB_6 , and the visible light is directed in an optical path to hit the MoS_2 sample at specific times, accounting for various factors. Thus, different diffraction patterns are recorded by the camera of the machine. Data on the electron diffraction patterns is collected from $t = -100$ to $t = 600$ picoseconds, where negative time is considered to be the time before photoexcitation and time $t = 0$ starts immediately before the excitation process. Data is collected for constant tilt and azimuthal angles as images on the picosecond scale.

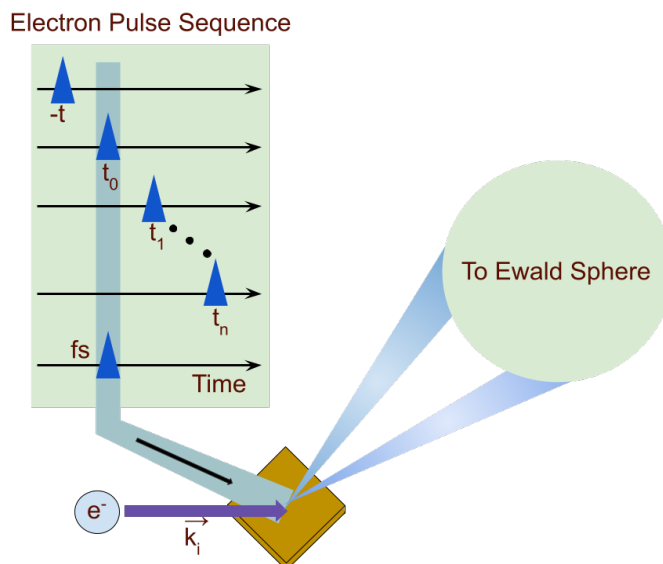


Fig. 19 The ultrafast electron diffraction setup, with the inclusion of the theoretical reciprocal space and Ewald sphere. An electron gun continues to probe while the crystal lattice is excited by the laser.

Acknowledgments

This work was conducted in the Yang Laboratory in the Department of Chemistry at the University of Houston, TX. We thank professor Ding-Shyue Yang and postdoctoral scholar Dr. Xing He for helping us collect data and understand the experiments, and we thank graduate student Larry Duong for consistently assisting us in learning concepts and progressing through our paper. Finally, we thank Jake Fallek for his contributions to the experiment.

References

- ¹Manzeli, S., Ovchinnikov, D., Pasquier, D., Yazyev, O. V., Kis, Andras. 2D transition metal dichalcogenides. *Nat Rev Mater*, **2**, 17033. (2017). doi:10.1038/natrevmats.2017.33
- ²Li, X., & Zhu, H. Two-dimensional MoS₂: Properties, preparation, and applications. *Journal of Materiomics*, **1**(1), 33–44. (2015). doi:10.1016/j.jmat.2015.03.003
- ³Ohtake, A., Yang, X. & Nara, J. Structure and morphology of 2H-MoTe₂ monolayer on GaAs(111)B grown by molecular-beam epitaxy. *npj 2D Mater Appl*, **6**, 35. (2022). doi:10.1038/s41699-022-00310-y
- ⁴Wang W, Yang C, Bai L, Li M, Li W. First-principles study on the structural and electronic properties of monolayer MoS₂ with S-vacancy under uniaxial tensile strain. *Nanomaterials*, **8**(2), 74. (2018). doi:10.3390/nano8020074
- ⁵Xiang, Y., Sun, X., Valdman, L., Zhang, F., Choudhury, T. H., Chubarov, M., Robinson, J. A., Redwing, J. M., Terrones, M., Ma, Y., Gao, L., Washington, M. A., Lu, T.-M., & Wang, G.-C. Monolayer MoS₂ on sapphire: An azimuthal reflection high-energy electron diffraction perspective. *2D Materials*, **8**(2), 025003. (2021). doi:10.1088/2053-1583/abce08
- ⁶Frigge, T., Hafke, B., Tinnemann, V., Witte, T., Horn-von Hoegen, M. Spot profile analysis and lifetime mapping in ultrafast electron diffraction: Lattice excitation of self-organized Ge nanostructures on Si(001). *Structural Dynamics*, **2**(3), 035101. (2015). doi:10.1063/1.4922023
- ⁷Ichimiya A., Cohen P. I. *Reflection high-energy electron diffraction*. Cambridge University Press: Cambridge, New York. (2004).

- ⁸Van Stokkum, I. H. M., Larsen, D. S., van Grondelle, R. Global and target analysis of time-resolved spectra. *Biochimica et Biophysica Acta (BBA) - Bioenergetics*, **1657**(2-3), 82–104. (2004). doi:10.1016/j.bbabi.2004.04.011
- ⁹Ruan, C.-Y., Yang, D.-S., & Zewail, A. H. Structures and dynamics of self-assembled surface monolayers observed by ultrafast electron crystallography. *Journal of the American Chemical Society*, **126**(40), 12797–12799. (2004). doi:10.1021/ja045441n
- ¹⁰Zewail, A. H. 4D ultrafast electron diffraction, crystallography, and microscopy. *Annual Review of Physical Chemistry*, **57**(1), 65–103. (2006). doi:10.1146/annurev.physchem.57.032905.104748
- ¹¹González Vallejo, I., Gallé, G., Arnaud, B., Scott, S. A., Lagally, M. G., Boschetto, D., Coulon, P.-E., Rizza, G., Houdellier, F., Bolloc'h, D. L., Faure, J. Observation of large multiple scattering effects in ultrafast electron diffraction on monocrystalline silicon. *Physical Review B*, **97**(5). (2018). doi:10.1103/physrevb.97.054302
- ¹²Yang, D.-S., Gedik, N., & Zewail, A. H. Ultrafast electron crystallography. 1. Nonequilibrium dynamics of nanometer-scale structures. *The Journal of Physical Chemistry C*, **111**(13), 4889–4919. (2007). doi:10.1021/jp067466+
- ¹³Wakabayashi, N., Smith, H. G., & Nicklow, R. M. Lattice dynamics of hexagonal MoS₂ studied by neutron scattering. *Physical Review B*, **12**(2), 659–663. (1975). doi:10.1103/physrevb.12.659
- ¹⁴Booker, I., Rahimzadeh Khoshroo, L., Woitok, J. F., Kaganer, V., Mauder, C., Behmenburg, H., Gruis, J., Heuken, M., Kalisch, H., Jansen, R. H. Dislocation density assessment via X-ray GaN rocking curve scans. *Physica Status Solidi (c)*, **7**(7-8), 1787–1789. (2010). doi:10.1002/pssc.200983615
- ¹⁵Li, C., Cui, D., Zhou, Y., Lu, H., Chen, Z., Zhang, D., & Wu, F. Asymmetric rocking curve study of the crystal structure orientations for BaTiO₃ thin films grown by pulsed laser deposition. *Applied Surface Science*, **136**(3), 173–177. (1998). doi:10.1016/s0169-4332(98)00342-0
- ¹⁶Yang, Ding-Shyue (Jerry). *Ultrafast electron crystallography: Principles and applications* [Doctoral dissertation, California Institute of Technology]. (2009). doi:10.7907/Y61P-2B24. <https://resolver.caltech.edu/CaltechETD:etd-05082009-170032>
- ¹⁷He, X., Chebl, M., & Yang, D.-S. Cross-examination of ultrafast structural, interfacial, and carrier dynamics of supported monolayer MoS₂. *Nano Letters*, **20**(3), 2026–2033. (2020). doi:10.1021/acs.nanolett.9b05344
- ¹⁸Eades, J. A. Laue zones: A clarification of nomenclature. *Ultramicroscopy*, **32**(2), 183. (1990). doi:10.1016/0304-3991(90)90037-m
- ¹⁹Pawlak, J., Przybylski, M., & Mitura, Z. An analysis of Kikuchi lines observed with a RHEED apparatus for a TiO₂-terminated SrTiO₃ (001) crystal. *Materials*, **14**(22), 7077. (2021). doi:10.3390/ma14227077
- ²⁰Chiappe, D., Scalise, E., Cinquanta, E., Grazianetti, C., van den Broek, B., Fanciulli, M., Houssa, M., Molle, A. Two-dimensional Si nanosheets with local hexagonal structure on a MoS₂ surface. *Advanced Materials*, **26**(13), 2096–2101. (2013). doi:10.1002/adma.201304783
- ²¹Ashcroft N., Mermin N. *Solid state physics*. Harcourt Incorporated, New York. (1976).
- ²²Wu, Chenyi. *Ordered structures of molecular assemblies at interfaces* [Doctoral dissertation, University of Houston]. Institutional Repository at the University of Houston. (2019). <https://uh-ir.tdl.org/handle/10657/5724>
- ²³Huang, H., Huang, C.-P., Zhang, C., Hong, X.-H., Zhang, X.-J., Qin, Y.-Q., & Zhu, Y.-Y. From Ewald sphere to Ewald shell in nonlinear optics. *Scientific Reports*, **6**(1). (2016). doi:10.1038/srep29365
- ²⁴Xiang, Y., Guo, F.-W., Lu, T.-M., & Wang, G.-C. Reflection high-energy electron diffraction measurements of reciprocal space structure of 2D materials. *Nanotechnology*, **27**(48), 485703. (2016). doi:10.1088/0957-4484/27/48/485703
- ²⁵Kim, H. W., Vinokurov, N. A., Baek, I. H., Oang, K. Y., Kim, M. H., Kim, Y. C., Jang, K.-H., Lee, K., Park, S. H., Park, S., Shin, J., Kim, J., Rotermund, F., Cho, S., Feurer, T., Jeong, Y. U. Towards jitter-free ultrafast electron diffraction technology. *Nature Photonics*, **14**(4), 245–249. (2019). doi:10.1038/s41566-019-0566-4
- ²⁶Liu, Z., Song, Y., Rajappan, A., Wang, E. N., & Preston, D. J. Temporal evolution of surface contamination under ultra-high vacuum. *Langmuir*, **38**(3), 1252–1258. (2022). doi:10.1021/acs.langmuir.1c03062